Essential Conditions for Dynamic Interference

Mehrdad Baghery, Ulf Saalmann, and Jan M. Rost
Max-Planck-Institut für Physik komplexer Systeme, Nöthnitzer Straße 38, 01187 Dresden, Germany
(Received 13 November 2016; published 5 April 2017)

We develop general quantitative criteria for dynamic interference, a manifestation of a double-slit interference in time which should be realizable with brilliant state-of-the-art high-frequency laser sources. Our analysis reveals that the observation of dynamic interference hinges upon maximizing the difference between the dynamic polarization of the initial bound and the final continuum states of the electron during the light pulse while keeping depletion of the initial state small. These two properties, Stark shift and depletion, can be determined from electronic structure calculations avoiding expensive propagation in time. Confirmed by numerical results, we predict that this is impossible for the hydrogen ground state but feasible for excited states; this has been exemplified for the case of the hydrogen $2p$ state.

DOI: 10.1103/PhysRevLett.118.143202

Interference is a basic concept ruling optical as well as quantum mechanical wave phenomena, most prominently realized through variations of the double-slit scenario, by means of photoelectron spectroscopy with short-wavelength radiation even on an atomic level [1–4]. The advent of intense laser pulses with a finite pulse length has contributed a new natural double-slit scenario in the time domain: A wave packet that is launched for some dynamic reason at a certain time of the raising part of the pulse, in principle, encounters the same laser envelope amplitude at a certain time during the falling part of the pulse, constituting a double slit in time. If the source for the wave packet has not changed between the two "slits," interference of both wave packets with maximal possible contrast results, depending on the time interval between the slits. This scenario was experimentally seen [5] and theoretically described [6] early on for bound-state population transfer with low-frequency pulses. It was touched upon in the context of stabilization study with the high-frequency Floquet theory for above-threshold ionization [7,8] to finally become topical under the name dynamic interference in the soft x-ray domain for femtosecond pulses [9,10]. Indeed, the breathtaking development of intense light sources towards attosecond pulse lengths [11] and x-ray frequencies [12] has tremendously broadened the parameter range available for light-matter interaction and, consequently, for the fundamental phenomenon of dynamic interference.

In order to trigger experiments and gain an understanding of the general phenomenon of dynamic interference, in the following, we will work out the parameter windows where dynamic interference is prominent on very different scales of time and energy. Formulating the relevant properties of the laser pulse and the target electron leads us to the appropriate theoretical framework for dynamic interference. Making use of the minimal analytical model described before [10], we will show that only its version in the (reduced) velocity gauge can be safely used. As it turns out, the same is true for numerical implementations of dynamic interference, although for different reasons. Surprisingly and in contrast to previous claims, we also find that ionization of hydrogen from its ground state does not exhibit dynamic interference, whereas ionization from an excited state does indeed result in dynamic interference.

The soft x-ray regime we will be mainly concerned with here (electron excess energies below 100 eV) is challenging from a theoretical point of view, since single-photon ionization in the vacuum ultraviolet regime *cannot* be taken as the indication for a standard perturbative light-matter coupling: First, there may be substantial depletion of the ionized state during the pulse, and second, multiphoton processes can be involved as indicated by appreciable dynamic Stark shifts (also referred to as ac Stark shifts) of energies. However, due to the weak transitions in the continuum, multiphoton interaction does not lead to substantial multiphoton ionization, in contrast to infrared or optical pulses [13].

For this intermediate regime of light-matter coupling, which is neither fully perturbative nor does it lead to multiphoton ionization, we will identify the two dimensionless parameters δ and γ accounting for the dynamic Stark shift and depletion of the initial state, respectively. The appearance of dynamic interference depends on a suitable ratio of these two parameters.

We start from the standard minimal-coupling Hamiltonian written in the velocity gauge:

$$\hat{H}^{\mathrm{vel}} = \frac{1}{2}[\hat{\mathbf{p}} + \boldsymbol{\mathcal{A}}(t)]^2 + V(\hat{\mathbf{r}}), \tag{1a}$$

where V is some external potential and

$$\boldsymbol{\mathcal{A}}(t) = \boldsymbol{\mathcal{A}}_0 g(t)\cos(\omega t) \tag{1b}$$

is the vector potential of the laser pulse with a Gaussian envelope $g(t) = \exp(-t^2/T^2)$. We use atomic units throughout the text unless noted otherwise. We represent solutions $|\psi(t)\rangle$ of the time-dependent Schrödinger equation for (1) with an expansion into field-free (bound and continuum) states φ_α:

$$|\psi(t)\rangle = e^{-(i/2)\int^t dt' \mathcal{A}^2(t')} \sum\!\!\!\!\!\!\int_\alpha |\varphi_\alpha\rangle e^{-iE_\alpha t} a_\alpha(t), \qquad (2)$$

where the exponential prefactor transforms away $\frac{1}{2}\mathcal{A}^2(t)$ appearing in (1a). We will call this new gauge the *reduced* velocity gauge. The index α comprises all quantum numbers defining the eigenstate, which in the case of continuum states are the energy E and the symmetry κ. The standard 1st-order time-dependent perturbation theory predicts the amplitude (of continuum states at energy E)

$$a_{E,\kappa} = -i\mathbf{p}_{E,\kappa} \int dt \mathcal{A}(t) e^{i[E-E_{\rm in}]t} a_{\rm in}(t) \qquad (3)$$

for ionization to a final energy E from initial energy $E_{\rm in}$. The dipole matrix elements $\mathbf{p}_{E,\kappa} \equiv \langle \varphi_{E,\kappa} | \hat{\mathbf{p}} | \varphi_{\rm in} \rangle$ connect the initial state $\varphi_{\rm in}$ to continuum states $\varphi_{E,\kappa}$ of energy E. Because of selection rules, only some of the matrix elements are nonzero. For the photoeffect, implying weak perturbations $\mathcal{A}(t)$, Eq. (3) allows for an explicit solution, since one may assume that $a_{\rm in}(t) = 1$ for all times.

For dynamic interference, however, the dynamic Stark shift and the depletion of the initial state become relevant. As long as the laser envelope varies slowly compared to the laser cycle, the system remains in an adiabatic regime where one may average the response of the system to the laser field over the laser cycle to arrive at a formulation solely expressed in terms of the laser envelope $g(t)$. Incorporated into (3), one obtains a modified coefficient $a_{\rm in}(t)$ which still allows for a solution (at least in terms of a stationary-phase approximation) as before [9,10]. Hereby, the phase of $a_{\rm in}$ becomes time dependent:

$$a_{\rm in}(t) = e^{-i\phi_{\rm in}^{\delta\gamma}(t)} \qquad (4a)$$

$$\phi_{\rm in}^{\delta\gamma}(t) = [\delta - i\gamma/2] E_p T G(t), \qquad (4b)$$

with the ponderomotive energy E_p and the dimensionless function G, respectively, defined by pulse parameters

$$E_p \equiv \frac{\mathcal{A}_0^2}{4} = \frac{I}{4\omega^2}, \qquad (4c)$$

$$G(t) \equiv \frac{1}{T} \int^t dt' g^2(t'). \qquad (4d)$$

The derivative $d\phi_{\rm in}^{\delta\gamma}/dt$ can be interpreted as the complex, frequency-dependent energy of the initial state in the laser pulse, proportional to the (peak) ponderomotive energy E_p. Thereby, δ accounts for the Stark shift Δ [the Stark shift is indeed the time derivative of the phase $\Delta(t) = \delta E_p T (d/dt) G(t) = \delta E_p(t)$ with $E_p(t) = E_p g^2(t)$], and the decay width γ accounts for the depletion. Both constants depend on the laser frequency ω and can be derived from the 2nd-order time-independent perturbation theory (see Sec. 1 of Supplemental Material [14]) or equally extracted from a numerical propagation [10]. Obviously, the minimal description (4) is valid only as long as the Stark shift and decay width are linear in E_p.

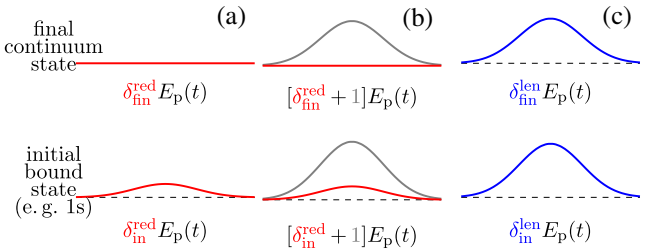

FIG. 1. Sketch showing the relation of the dynamic Stark shifts $\Delta(t)$ of both the initial bound and final continuum states for (a) the reduced velocity gauge $\hat{H}^{\rm red} = \frac{1}{2}\hat{\mathbf{p}}^2 + \mathcal{A}(t)\hat{\mathbf{p}} + V(\hat{\mathbf{r}})$, (b) the velocity gauge $\hat{H}^{\rm vel} = \frac{1}{2}[\hat{\mathbf{p}} + \mathcal{A}(t)]^2 + V(\hat{\mathbf{r}})$, and (c) the length gauge $\hat{H}^{\rm len} = \frac{1}{2}\hat{\mathbf{p}}^2 + V(\hat{\mathbf{r}}) - \frac{d}{dt}\mathcal{A}(t)\cdot\hat{\mathbf{r}}$, respectively. See also Sec. 2 of Supplemental Material [14].

In Eq. (4), the dynamic Stark shift has been introduced only to the initial state but not to the final state in the continuum. This is legitimate only in the reduced velocity gauge, where each state has just an intrinsic dynamic Stark shift as shown in Fig. 1(a), with the one for the continuum being in general negligible. This also applies to the velocity gauge [Fig. 1(b)], where all states have an *additive* ponderomotive shift, which can be easily removed by a global phase in the wave function as done in Eq. (2). By contrast, in the length gauge the ponderomotive shift *cannot* be easily separated, as indicated in Fig. 1(c). There, to a good approximation [17], the Stark shift of continuum electrons is given by the ponderomotive energy. Consequently, the intrinsic Stark shift of any continuum state in the reduced velocity gauge is rather small and negligible, rendering the description with Eq. (4) adequate.

As just emphasized, in the length gauge the (trivial) ponderomotive shift cannot be split off the initial or final states and therefore has to be covered by any convergent numerical calculation, which is typically much more demanding than in the velocity gauge (e.g., many more partial waves are required). This is the reason why it has been noted in long-wavelength strong-field physics that the velocity gauge is preferable for numerical calculations [18,19].

From Fig. 1, one obtains an intuitive understanding regarding the mechanism behind dynamic interference independent of the gauge: The initial-state energy increased

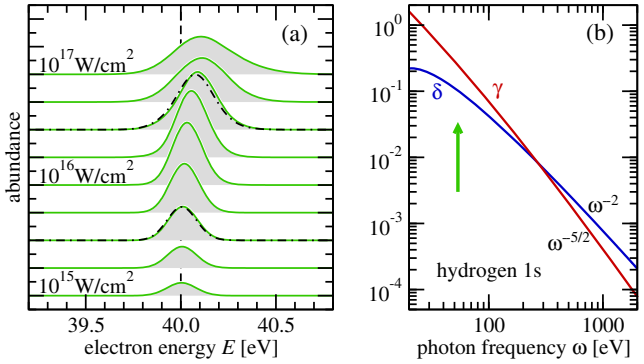

FIG. 2. (a) Photoelectron spectra for $1s$ hydrogen exposed to 10 fs pulses with a carrier frequency of $\omega = 53.60$ eV for intensities $I_k = 10^{k/4} \times 10^{15}$ W/cm^2 with $k = 0, 1, \ldots, 8$. The dashed line marks the energy $E_\omega = E_{1s} + \omega = 40$ eV. The result of the minimal model (4) is shown for two intensities by dot-dashed lines. (b) Dimensionless parameters $\delta(\omega)$ and $\gamma(\omega)$ for the hydrogen $1s$ state as introduced in Eq. (4) and defined in detail in Sec. 1 of Supplemental Material [14]. The asymptotic behavior of them for $\omega \to \infty$ is given for both [20]. The green arrow marks the frequency $\omega = 53.6$ eV used in the left panel and in previous publications [9,10].

by ω for single-photon absorption may intersect the energy E of the final state at two points (in time). These time instants are stationary-phase points where the time derivative of the phase in the integral (3) vanishes; hence, the amplitudes at these two dominate the integral constituting the two-slit scenario. Dynamic interference will be most pronounced if the Stark shifts of initial and final states are very different. Quantitative details as well as the possibility for dynamic interference in the first place depend, of course, on the parameters entering the phase, namely, the electronic response properties $\delta(\omega)$ and $\gamma(\omega)$ in connection with the pulse properties E_p and T, which we will analyze next.

From the minimal model (4), it is easy to see that two conditions must be fulfilled for dynamic interference: (i) The Stark shift must be larger than the bandwidth of the pulse with length T in order to be energetically resolved, and (ii) depletion should be sufficiently weak in order to have ionization in the rising *and* falling wings of the pulse. In order to quantify these conditions, we note that the bandwidth of the pulse (1b) is $\sqrt{2}/T$ and that $G(0) = \sqrt{\pi/2}$. Thus, on one hand, condition (i) is satisfied if

$$\delta E_p > \sqrt{2}/T \quad \text{or} \quad E_p T > \frac{\sqrt{2}}{\delta}. \tag{5}$$

On the other hand, condition (ii) is fulfilled if

$$\frac{\gamma}{2} E_p T G(0) < 1 \quad \text{or} \quad E_p T < \frac{\sqrt{2/\pi}}{\gamma}. \tag{6}$$

These two conditions give lower and upper limits for the product $E_p T$. Apparently, they can be met simultaneously —thus allowing for dynamic interference—only if

$$\delta > \sqrt{\pi}\gamma, \tag{7}$$

which implies that in the competition between the Stark shift and depletion the former should dominate. This condition holds for any atom or molecule. As a consequence, we can predict the laser parameters for which one will observe dynamic interference, provided the response parameters $\delta(\omega)$ and $\gamma(\omega)$ are known. They are shown in Fig. 2(b) for the ground state of hydrogen as an example.

Having condition (7) in mind, one sees from Fig. 2(b) that this requires frequencies larger than $\tilde{\omega} = 265$ eV [21], where $\gamma(\tilde{\omega}) = \delta(\tilde{\omega})$ holds. This is confirmed by the numerical photoabsorption spectra in Fig. 2(a) determined by the direct propagation of the time-dependent Schrödinger equation in the (reduced) velocity gauge for the photon frequency ω marked by the green arrow in Fig. 2(b). Numerical details are given in Sec. 3 of Supplemental Material [14]; the parameters used are $\ell_{\max} = 4$, $r_{\max} = 3000 a_0$, $n = 3000$, and $E_{\max} \approx 134$ eV. As one can see from Fig. 2(a), the spectrum has a single photoelectron peak which gets Stark-shifted and broadened for increasing intensities while keeping the pulse length fixed at $T = 10$ fs. The results have been confirmed with two other packages [22,23] for the numerical propagation of the time-dependent Schrödinger equation.

In contradiction to these results, dynamic interference has been reported for the hydrogen ground state [9,10,24,25]. Even more puzzling, the numerical findings (obtained in the length gauge) seem to be supported by corresponding results from the minimal model in the length gauge appearing in the same papers. It is very rare and unfortunate that two independent mistakes, both related to a faulty usage of the length gauge, one in the model and one in the numerical calculation, should lead to agreeing results, seemingly reassuring the findings regarding dynamic interference [26].

The analytical mistake is easy to identify and originates from using the minimal model (4) in the length gauge but leaving out the Stark shift in the continuum state [see Fig. 1(c)]. Thereby, the difference between the time-dependent energies of initial and final states is artificially increased, leading to the appearance of stationary-phase points of the integrand in (4) at the wrong intensities. The numerical calculations were carried out in the length gauge with a limited number of partial waves, not enough to properly describe the ponderomotive motion of the electron. This parallels the mistake in the analytical model, where the ponderomotive energy dependence was left out and therefore leads to the accidental agreement of numerical and analytical calculations in those papers [9,10,24,25]. A detailed comparison of numerical calculations in the length and velocity gauges for different maximal angular

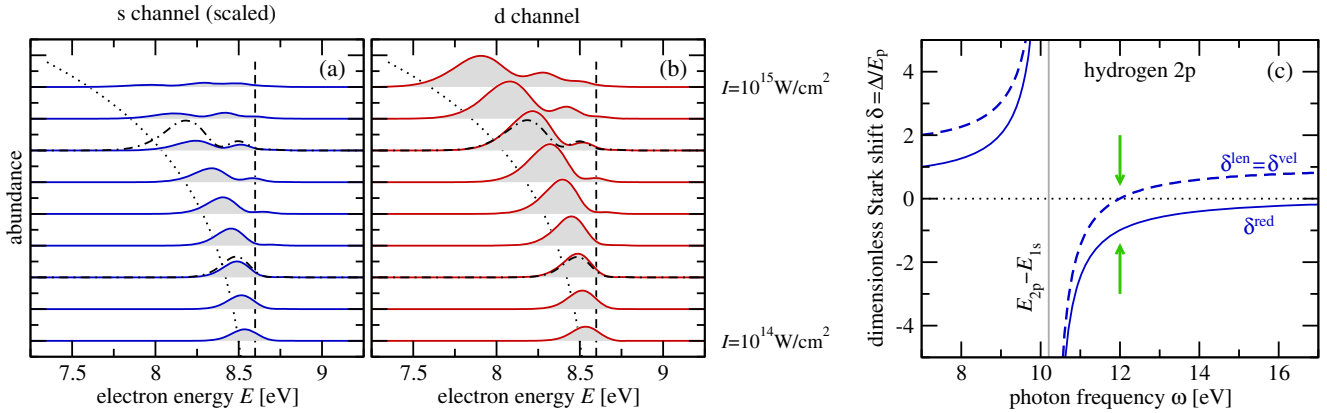

FIG. 3. Photoelectron spectra for 10 fs pulses with a carrier frequency of $\omega = 12$ eV for hydrogen in the $2p$ state. Ionization into the s channel (a) and the d channel (b) is shown. The intensities from bottom to top are $I_k = 10^{k/8} \times 10^{14}$ W/cm^2 with $k = 0, 1, \ldots, 8$. The dashed line marks the energy $E_\omega = E_{2p} + \omega = 8.59875$ eV, and the dotted line interpolates between the energies $E_{\omega,k} = E_{2p} + \omega - E_p(I_k)$. The s channel is scaled by the factor f in order to make the height of the peak equal in the perturbative limit: $f = |\mathbf{p}_{E_\omega,s}|/|\mathbf{p}_{E_\omega,d}| \approx 6.137$. The result of the minimal model (4) is shown for two intensities by dot-dashed lines. (c) Dimensionless Stark shift δ for the $2p$ state of hydrogen as a function of the photon frequency ω in units of the ponderomotive energy $\delta \equiv \Delta/E_p$. We show $\delta^{\text{len}} = \delta^{\text{vel}}$ (blue solid curves) and $\delta^{\text{red}} = \delta^{\text{vel}} - 1$ (blue dashed curves); cf. Sec. 2 of Supplemental Material [14]. The green arrow marks the photon frequency $\omega = 12$ eV, where the Stark shift vanishes and which was used in the two left panels. The Stark shift diverges at the transition energy $E_{2p} - E_{1s}$ (gray solid line).

momenta can be found in Sec. 3 of Supplemental Material [14].

Extrapolating from the conditions for dynamic interference in ionizing hydrogen, it seems very difficult to realize this phenomenon with state-of-the art laser systems. Yet, this can be easily achieved starting from the $2p$ excited state, which at the same time highlights the relevance of considering the proper Stark shifts. Starting from $2p$ and choosing appropriate intensities and frequencies of the laser, we can prepare an effective initial state which has no Stark shift in the length gauge (or a large negative Stark shift in the reduced velocity gauge). This implies a large difference in the Stark shifts between the continuum and initial bound states and therefore offers excellent conditions for dynamic interference.

At a frequency of $\omega = 12$ eV, the dynamic Stark shift of the $2p$ state vanishes (in the length and velocity gauges) and is therefore given by $\Delta(t) = -E_p(t)$ in the reduced velocity gauge, as can be seen in Fig. 3(c). At this frequency, the coupling to the $1s$ state fully compensates the coupling to all other states such that the polarizability and the Stark shift vanish. We have performed a propagation with the same parameters as before and obtained the spectra shown in Figs. 3(a) and 3(b); cf. details in Sec. 2 of Supplemental Material [14]. Since we start from a p state, photoelectrons are emitted into s and d channels, where the yield for the latter is larger due to the larger dipole matrix element. However, qualitatively, both angular momentum channels exhibit the same behavior for increasing intensities I. For low intensities, the spectrum is Gaussian-shaped and slightly redshifted with respect to $E_\omega = E_{2p} + \omega$. This shift increases with larger I, and for $I \gtrsim 5 \times 10^{14}$ W/cm^2 one clearly sees dynamic interference in both channels. We note in passing that, according to earlier publications [9,10], one would not expect any dynamic interference at all here. Moreover, in contrast to the blueshift predicted previously, we observe a redshift increasing with intensity which follows directly from $\Delta(t) < 0$ mentioned above.

In summary, by formulating single-photon ionization in the 1st-order time-dependent perturbation theory with phases obtained from the 2nd order, we have derived quantitative conditions under which dynamic interference can occur. The approach is tailored towards the dynamic regime of nonperturbative single-photon ionization, characteristic of interactions with intense soft x rays, and has allowed for the separation of the frequency-dependent response of the electronic system in terms of Stark shift $\delta(\omega)$ and depletion $\gamma(\omega)$ and the time-dependent laser pulse envelope. This separation facilitates the determination of the electronic response by electronic structure calculations and helps to accurately assess experimental conditions for dynamic interference.

[1] D. Akoury *et al.*, The simplest double slit: Interference and entanglement in double photoionization of H_2, Science **318**, 949 (2007).

[2] L. Argenti *et al.*, Double-slit experiment with a polyatomic molecule: Vibrationally resolved C 1s photoelectron spectra of acetylene, New J. Phys. **14**, 033012 (2012).

[3] R. K. Kushawaha, M. Patanen, R. Guillemin, L. Journel, C. Miron, M. Simon, M. N. Piancastelli, C. Skates, and P. Decleva, From double-slit interference to structural

information in simple hydrocarbons, Proc. Natl. Acad. Sci. U.S.A. **110**, 15201 (2013).
[4] X.-J. Liu, Q. Miao, F. Gel'mukhanov, M. Patanen, O. Travnikova, C. Nicolas, H. Ågren, K. Ueda, and C. Miron, Einstein-Bohr recoiling double-slit gedanken experiment performed at the molecular level, Nat. Photonics **9**, 120 (2015).
[5] R. R. Jones, Interference Effects in the Multiphoton Ionization of Sodium, Phys. Rev. Lett. **74**, 1091 (1995).
[6] K. J. Schafer and K. C. Kulander, Theory of resonant multiphoton population transfer in xenon, Laser Phys. **7**, 740 (1997).
[7] K. Toyota, O. I. Tolstikhin, T. Morishita, and S. Watanabe, Siegert-state expansion in the Kramers-Henneberger frame: Interference substructure of above-threshold ionization peaks in the stabilization regime, Phys. Rev. A **76**, 043418 (2007).
[8] K. Toyota, O. I. Tolstikhin, T. Morishita, and S. Watanabe, Interference substructure of above-threshold ionization peaks in the stabilization regime, Phys. Rev. A **78**, 033432 (2008).
[9] P. V. Demekhin and L. S. Cederbaum, Dynamic Interference of Photoelectrons Produced by High-Frequency Laser Pulses, Phys. Rev. Lett. **108**, 253001 (2012).
[10] P. V. Demekhin and L. S. Cederbaum, ac Stark effect in the electronic continuum and its impact on the photoionization of atoms by coherent intense short high-frequency laser pulses, Phys. Rev. A **88**, 043414 (2013).
[11] F. Krausz and M. Ivanov, Attosecond physics, Rev. Mod. Phys. **81**, 163 (2009).
[12] B. W. J. McNeil and N. R. Thompson, Xray free-electron lasers, Nat. Photonics **4**, 814 (2010).
[13] C. J. Joachain, N. J. Kylstra, and R. M. Potvliege, *Atoms in Intense Laser Fields* (Cambridge University Press, Cambridge, England, 2011).
[14] See Supplemental Material at http://link.aps.org/supplemental/10.1103/PhysRevLett.118.143202 for a compilation of some basic analytical expressions and details of the numerical propagation, which contains additional references [15,16].
[15] M. H. Mittleman, *Introduction to the Theory of Laser-Atom Interactions* (Plenum, New York, 1993).
[16] R. Jackiw, Quantum-Mechanical Sum Rules, Phys. Rev. **157**, 1220 (1967).
[17] N. B. Delone and V. P. Krainov, *Multi-photon Processes in Atoms* (Springer, Berlin, 2000).
[18] E. Cormier and P. Lambropoulos, Optimal gauge and gauge invariance in non-perturbative time-dependent calculation of above-threshold ionization, J. Phys. B **29**, 1667 (1996).
[19] H. G. Muller, An efficient propagation scheme for the time-dependent Schrödinger equation in the velocity gauge, Laser Phys. **9**, 138 (1999).
[20] M. Gavrila, in *Atoms in Intense Laser Fields*, edited by M. Gavrila (Academic, San Diego, 1992).
[21] For $\omega \gg \tilde{\omega}$, the absolute values are very small and the required intensities are accordingly large. We have verified numerically our prediction by numerically calculating the spectrum at $\omega = 1$ keV, which indeed showed an interference structure.
[22] D. Bauer and P. Koval, Q PROP: A Schrödinger-solver for intense laser-atom interaction, Comput. Phys. Commun. **174**, 396 (2006).
[23] S. Patchkovskii and H. G. Muller, Simple, accurate, and efficient implementation of 1-electron atomic time-dependent Schrödinger equation in spherical coordinates, Comput. Phys. Commun. **199**, 153 (2016).
[24] P. V. Demekhin, D. Hochstuhl, and L. S. Cederbaum, Photoionization of hydrogen atoms by coherent intense high-frequency short laser pulses: Direct propagation of electron wave packets on large spatial grids, Phys. Rev. A **88**, 023422 (2013).
[25] C. Yu, N. Fu, G. Zhang, and J. Yao, Dynamic Stark effect on XUV-laser-generated photoelectron spectra: Numerical experiment on atomic hydrogen, Phys. Rev. A **87**, 043405 (2013).
[26] In a recent paper [A. N. Artemyev, A. D. Müller, D. Hochstuhl, L. S. Cederbaum, and P. V. Demekhin, Dynamic interference in the photoionization of He by coherent intense high-frequency laser pulses: Direct propagation of the two-electron wave-packets on large spatial grids, Phys. Rev. A **93**, 043418 (2016)], the authors were more fortunate: Here, the technically erroneous omission of the ponderomotive shift in the continuum part of the final singly ionized two-electron state is justified thanks to the much larger Stark shift of its bound part, in both the model and the numerical propagation.

Supplement for "Essential conditions for dynamic interference"

Mehrdad Baghery, Ulf Saalmann & Jan M. Rost

A detailed derivation of some (largely known) basic analytical expressions is provided. Firstly, we give explicit expressions for the two dimensionless parameters δ and γ describing respectively the dynamic Stark shift and the depletion of some state in a high-frequency laser pulse, followed by their asymptotic behaviour. Secondly, we show how the Stark shifts in different gauges are related. Thirdly, we outline the numerical procedure for propagation of the TDSE, and stress convergence problems in the length gauge by comparing the results of a few systematic simulations (with an increasing number of partial waves included in the propagation) in the velocity and length gauges.

1 Stark shift and depletion in single-photon ionization

In order to explain the notation used in the text[1], in this section we will describe the Stark shift and the depletion of an initial state upon irradiation with a high-frequency laser pulse. The ideas presented here largely follow those presented before [1], followed by further definitions and a general discussion.

The wavefunction evolving according to the time-dependent Schrödinger equation

$$\mathrm{i}\frac{\partial}{\partial t}\big|\psi(t)\big\rangle = \hat{H}(t)\big|\psi(t)\big\rangle \quad \text{with} \quad \hat{H}(t) = \frac{1}{2}\big[\hat{\mathbf{p}} + \boldsymbol{\mathcal{A}}(t)\big]^2 + V(\hat{\mathbf{r}}) \\ \text{and} \quad \boldsymbol{\mathcal{A}}(t) = \boldsymbol{\mathcal{A}}_0\, g(t)\cos(\omega t) \tag{S1}$$

can be expanded in terms of field-free states, cf. ansatz (2) in the text. The amplitude of the initially occupied state φ_{in}, and all the bound/continuum states φ_α having a non-vanishing coupling $\mathbf{p}_\alpha = \langle\varphi_\alpha|\hat{\mathbf{p}}|\varphi_{\mathrm{in}}\rangle$ with the initial state respectively reads

$$\mathrm{i}\frac{\mathrm{d}}{\mathrm{d}t}a_{\mathrm{in}}(t) = g(t)\sum\!\!\!\!\!\!\int_\alpha \boldsymbol{\mathcal{A}}_0\cdot\frac{\mathbf{p}_\alpha{}^*}{2}\sum_\pm \mathrm{e}^{\mathrm{i}[E_{\mathrm{in}}\pm\omega-E_\alpha]t}a_\alpha(t), \tag{S2a}$$

$$\mathrm{i}\frac{\mathrm{d}}{\mathrm{d}t}a_\alpha(t) = g(t)\,\boldsymbol{\mathcal{A}}_0\cdot\frac{\mathbf{p}_\alpha}{2}\sum_\pm \mathrm{e}^{\mathrm{i}[E_\alpha\pm\omega-E_{\mathrm{in}}]t}a_{\mathrm{in}}(t). \tag{S2b}$$

Assuming that the envelope changes slowly, i. e. $\frac{\mathrm{d}}{\mathrm{d}t}g(t) \approx 0$, which implies $\frac{\mathrm{d}}{\mathrm{d}t}a_{\mathrm{in}}(t) \approx 0$, one can solve Eq. (S2b) approximately to get

$$a_\alpha(t) \approx -g(t)\,\boldsymbol{\mathcal{A}}_0\cdot\frac{\mathbf{p}_\alpha}{2}\sum_\pm \frac{\mathrm{e}^{\mathrm{i}[E_\alpha-E_{\mathrm{in}}\pm\omega]t}}{E_\alpha-E_{\mathrm{in}}\pm\omega}a_{\mathrm{in}}(t). \tag{S3}$$

This can be in turn used in Eq. (S2a) to get the following equation for the amplitude of the initially occupied state

$$\frac{\mathrm{d}}{\mathrm{d}t}a_{\mathrm{in}}(t) = -\mathrm{i}E_{\mathrm{p}}(t)\big[\delta-\mathrm{i}\gamma/2\big]a_{\mathrm{in}}(t) \qquad \text{with} \quad E_{\mathrm{p}}(t) \equiv \frac{\mathcal{A}_0{}^2}{4}g^2(t), \tag{S4a}$$

[1]Here and in the following we use "text" when referring to the text of main manuscript.

where terms with $\mathrm{e}^{\pm \mathrm{i}2\omega t}$ have been neglected and the following definitions have been used

$$\delta \equiv -\sum\!\!\!\!\!\!\int_{\alpha} \sum_{\pm} \frac{\widetilde{p}_\alpha{}^2}{E_\alpha - E_{\mathrm{in}} \pm \omega} = \sum\!\!\!\!\!\!\int_{\alpha} \widetilde{p}_\alpha{}^2 \frac{2[E_\alpha - E_{\mathrm{in}}]}{\omega^2 - [E_\alpha - E_{\mathrm{in}}]^2} \tag{S4b}$$

$$\gamma \equiv 2\pi \int \mathrm{d}E_\alpha \, \delta\big(E_\alpha - [E_{\mathrm{in}} + \omega]\big) \, \widetilde{p}_\alpha{}^2 = 2\pi \, \widetilde{p}_\omega{}^2 \quad \text{with } E_\omega = E_{\mathrm{in}} + \omega \tag{S4c}$$

$$\widetilde{p}_\alpha \equiv \frac{\boldsymbol{\mathcal{A}}_0}{|\boldsymbol{\mathcal{A}}_0|} \cdot \mathbf{p}_\alpha, \tag{S4d}$$

with the integral part of Eq. (S4b) being understood as Cauchy principal value.

Such equations have been derived before [1], but here δ and γ are defined slightly differently such that they are solely determined by the system (and the frequency). In particular, we have taken out the instantaneous ponderomotive energy $E_{\mathrm{p}}(t)$ which depends on time through the pulse envelope $g(t)$ as defined in Eq. (S4a).

1.1 Asymptotic behavior and condition for dynamic interference

The asymptotic behavior of δ and γ at large frequencies ω is given by

$$\delta \approx 2 \sum_{\alpha} \frac{[E_\alpha - E_{\mathrm{in}}] \, \widetilde{p}_\alpha{}^2}{\omega^2} \sim \omega^{-2} \tag{S5a}$$

$$\gamma \sim \sqrt{\omega} \Big[\omega \frac{8\sqrt{2\omega}}{[1+2\omega]^3} \Big]^2 \sim \omega^{-5/2}. \tag{S5b}$$

where in the first step of Eq. (S5a) we have restricted the sum to bound states since their coupling matrix elements are much larger than those of the continuum states. In the second step we have assumed $E_\alpha - E_{\mathrm{in}} \ll \omega$. In order to get Eq. (S5b), we note that at high frequencies ω (and thus high energies E_α) the electron can be considered free and therefore its radial wavefunction becomes $\varphi_\alpha \sim [2E_\alpha]^{1/4} j_1(\sqrt{2E_\alpha} r) \approx [2\omega]^{1/4} j_1(\sqrt{2\omega} r)$, with j_1 being the 1st-order spherical Bessel function. This allows for an easy analytical integration with the result shown above. The asymptotic behavior (S5) has been derived by means of high-frequency Floquet theory before [2].

As becomes clear from these considerations, one always ends up with $\gamma < \delta$ in the limit of $\omega \to \infty$ regardless of the system. In other words, for any system there is always a crossover frequency $\widetilde{\omega}$, however large, above which $\gamma(\omega) < \delta(\omega)$. Thus — in principle — dynamic interference can be observed for appropriate laser parameters.

Considering a hydrogen-like atom with nuclear charge Z, one gets related quantities

$$\delta_Z(\omega) = Z^{-4} \, \delta(Z^2 \omega), \quad \gamma_Z(\omega) = Z^{-4} \, \gamma(Z^2 \omega) \tag{S6}$$

by simple scaling arguments. Visibly the transition to $\delta_Z(\omega) > \sqrt{\pi} \, \gamma_Z(\omega)$ occurs for $Z > 1$ at a Z^2–times larger frequency and is connected with a Z^4–times larger product $E_{\mathrm{p}} \, T$, cf. Eqs. (5) and (6) in the text.

2 Dynamic Stark shift

We summarize formulas for the dynamic Stark shift (often referred to as AC Stark shift) and discuss the Stark of the ground and an excited state of the hydrogen atom.

2.1 Length vs. velocity gauge

Given the three Hamiltonians [3]

$$\hat{H}^{\mathrm{red}} = \frac{1}{2}\hat{\mathbf{p}}^2 + \boldsymbol{\mathcal{A}}(t)\hat{\mathbf{p}} + V(\hat{\mathbf{r}}) \tag{S7a}$$

$$\hat{H}^{\mathrm{vel}} = \frac{1}{2}\big[\hat{\mathbf{p}} + \boldsymbol{\mathcal{A}}(t)\big]^2 + V(\hat{\mathbf{r}}) \tag{S7b}$$

$$\hat{H}^{\mathrm{len}} = \frac{1}{2}\hat{\mathbf{p}}^2 + V(\hat{\mathbf{r}}) - \frac{\mathrm{d}}{\mathrm{d}t}\boldsymbol{\mathcal{A}}(t)\cdot\hat{\mathbf{r}} \tag{S7c}$$

and the initial conditions $\big|\psi^{\mathrm{len}}(-\infty)\big\rangle = \big|\psi^{\mathrm{vel}}(-\infty)\big\rangle = \big|\psi^{\mathrm{red}}(-\infty)\big\rangle$, the solutions of the time-dependent Schrödinger equation for $\xi = \mathrm{len}, \mathrm{vel}, \mathrm{red}$

$$\mathrm{i}\frac{\partial}{\partial t}\big|\psi^{\xi}(t)\big\rangle = \hat{H}^{\xi}\big|\psi^{\xi}(t)\big\rangle \tag{S8}$$

are connected by

$$\big|\psi^{\mathrm{vel}}(t)\big\rangle = \mathrm{e}^{-\frac{\mathrm{i}}{2}\int^t \mathrm{d}t' \boldsymbol{\mathcal{A}}^2(t')}\big|\psi^{\mathrm{red}}(t)\big\rangle, \tag{S9a}$$

$$\big|\psi^{\mathrm{len}}(t)\big\rangle = \mathrm{e}^{+\mathrm{i}\boldsymbol{\mathcal{A}}(t)\cdot\hat{\mathbf{r}}}\big|\psi^{\mathrm{vel}}(t)\big\rangle. \tag{S9b}$$

Note that $\big|\psi^{\mathrm{len}}(t_*)\big\rangle = \big|\psi^{\mathrm{vel}}(t_*)\big\rangle$ every time when $\mathcal{A}(t_*) = 0$, i.e. both states agree periodically. $\big|\psi^{\mathrm{vel}}(t)\big\rangle$ and $\big|\psi^{\mathrm{red}}(t)\big\rangle$ differ only by a trivial phase $\mathrm{e}^{-\frac{\mathrm{i}}{2}\int^t \mathrm{d}t' \mathcal{A}^2(t')}$ introduced in Eq. (2) of the text.

By means of the 2nd-order perturbation theory one can calculate the Stark shift of an eigenstate φ_* in terms of all (bound and continuum) eigenstates in the three cases as follows [3], cf. also Eq. (S4b) above,

$$\Delta^{\mathrm{red}}(t) = E_{\mathrm{p}}(t) \sum\!\!\!\!\!\!\int_{\alpha} \big|\big\langle\varphi_\alpha\big|\hat{\mathbf{p}}\big|\varphi_*\big\rangle\big|^2 \frac{2E_{\alpha*}}{\omega^2 - {E_{\alpha*}}^2}, \tag{S10a}$$

$$\Delta^{\mathrm{vel}}(t) = \Delta^{\mathrm{red}}(t) + E_{\mathrm{p}}(t), \tag{S10b}$$

$$\Delta^{\mathrm{len}}(t) = E_{\mathrm{p}}(t) \sum\!\!\!\!\!\!\int_{\alpha} \big|\big\langle\varphi_\alpha\big|\hat{\mathbf{r}}\big|\varphi_*\big\rangle\big|^2 \frac{2E_{\alpha*}}{1 - {E_{\alpha*}}^2/\omega^2}. \tag{S10c}$$

where the abbreviation $E_{\alpha*} \equiv E_\alpha - E_*$ is used. As above, $E_{\mathrm{p}}(t)$ is the instantaneous ponderomotive energy which changes in time because of the pulse envelope $g(t)$.

By means of the identity $\langle\varphi_\alpha|\hat{\mathbf{p}}|\varphi_*\rangle = \mathrm{i}E_{\alpha*}\langle\varphi_\alpha|\hat{\mathbf{r}}|\varphi_*\rangle$ for the matrix elements and the TRK sum rule [4], $1 = 2\sum_\alpha E_{*\alpha}|\langle\varphi_\alpha|\hat{\mathbf{r}}|\varphi_*\rangle|^2$, it is easy to show that $\Delta^{\mathrm{vel}} = \Delta^{\mathrm{len}}$. It turns out, the Stark shift in the length gauge always contains (in a non-separable way) the ponderomotive shift $E_{\mathrm{p}}(t)$, whereas in the velocity gauge the ponderomotive shift can be easily taken out simply by neglecting $\frac{1}{2}\mathcal{A}^2(t)$ in the Hamiltonian (S7b) and using (S7a) instead. All three expressions (S10) are shown schematically in Fig. 1 of the text.

The Stark shifts in the various gauges are written in (S10) in a form that suggests

$$\Delta^{\xi}(t) = \delta^{\xi}\, E_{\mathrm{p}}(t), \tag{S11}$$

where again $\xi = \mathrm{len}, \mathrm{vel}, \mathrm{red}$, and δ^{ξ} are the dimensionless parameters introduced in Sec. 1 above and used throughout the text.

2.2 Hydrogen atom

The dynamic Stark shift of the hydrogen ground-state is typically positive at large frequencies $\omega > |E_*|$ with E_* being the ground-state energy. This can be easily seen in Eqs. (S10) where the dominating states (those with $E_\alpha \approx E_*$ which also happen to have the largest dipole matrix elements) have a positive denominator as well as a positive numerator, whereas contributions from states with a negative denominator ($E_\alpha \gtrsim E_* + \omega$) are suppressed in two ways: firstly these states have small dipole matrix elements, and secondly they are largely canceled out by those with $E_\alpha \lesssim E_* + \omega$. Therefore the sketch shown in Fig. 1 of the text does not just apply to hydrogen in the 1s-state but is typically for any ground-state atom.

The 2p-state has a negative term in the sum from the coupling to the 1s-state for frequencies $\omega > E_{2p} - E_{1s}$ (negative numerator and positive denominator). Depending on how close ω is to the 1s-2p transition energy, the total sum (and thus the observed dynamic Stark shift) can be negative or positive. This allows one, by choosing $\omega = 12\,\text{eV}$, to have $\delta^{\text{len}} = \delta^{\text{vel}} = 0$ and consequently $\Delta^{\text{len}}(t) = \Delta^{\text{vel}}(t) = 0$. Hence, the effective Stark shift is $\delta^{\text{red}} = -1$, and therefore $\Delta^{\text{red}}(t) = -E_{\text{p}}(t)$, cf. (S10b). This means that in this case the (negative) Stark shift *increases* the transition energy from the 2p to any continuum state by the instantaneous ponderomotive energy $E_{\text{p}}(t)$. This explains the red-shift observed while increasing the intensity as seen in Fig. 3 of the text.

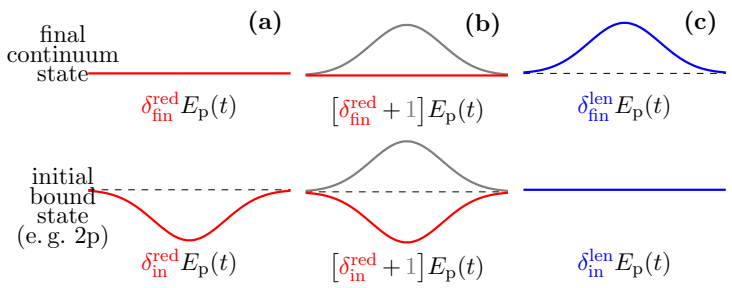

Figure S1: Sketch, analogous to Fig. 1 in the text, showing the relation between the dynamic Stark shift of the initial and final states in either reduced velocity, velocity or length gauge for a state with vanishing Stark shift (e. g. for the 2p-state of hydrogen at $\omega = 12\,\text{eV}$, where $\delta^{\text{red}}_{\text{in}} \approx -1$, $\delta^{\text{red}}_{\text{fin}} \approx 0$, $\delta^{\text{len}}_{\text{in}} \approx 0$ and $\delta^{\text{len}}_{\text{fin}} \approx +1$).

3 Time-dependent Schrödinger equation

In this section we will give details of the numerical calculations presented in the text.

3.1 Numerical propagation and spectra

The lowest n field-free states of each angular momentum $\ell = 0 \ldots \ell_{\text{max}}$ are calculated numerically by means of the Numerov method in a finite box $r = 0 \ldots r_{\text{max}}$ of grid spacing $\delta r = 0.01\,\text{a}_0$. The size of the box r_{max} is chosen such that the continuum wave-packet does not reach the box boundary within the propagation time ($r_{\text{max}} \approx 2000 \ldots 4000\,\text{a}_0$). The energy of the highest state for each angular momentum can be estimated as $E_{\text{max}} \approx n^2\pi^2/2{r_{\text{max}}}^2$ (e. g. for $n = 3000$ and $r_{\text{max}} = 3000\,\text{a}_0$ it is $E_{\text{max}} \approx 134\,\text{eV}$).

The dipole coupling matrix between states j and j', where $|\ell_j - \ell_{j'}| = 1$, with radial functions φ_j and $\varphi_{j'}$ is calculated as $p_{jj'} = \text{i}[E_j - E_{j'}] \frac{\ell}{\sqrt{4\ell^2-1}} \langle \varphi_j | r | \varphi_{j'} \rangle$ with $\ell = \max(\ell_j, \ell_{j'})$. The time-dependent

Schrödinger equation can be written in terms of these couplings as

$$\mathrm{i}\dot{a}_j(t) = \sum_{j'} \left[E_j\delta_{jj'} + \mathcal{A}(t)\, p_{jj'}\right] a_{j'}(t), \tag{S12}$$

whereby the numerical propagation is facilitated by the fact that the matrix $p_{jj'}$ has a block structure.

The electron energy spectrum for a certain channel, i.e. a certain angular momentum, is obtained using the sum

$$P_\ell(E) = \frac{1}{\sqrt{\pi}\,\sigma_E} \sum_{j(\in\ell)} \left|a_j(t_\mathrm{fin})\right|^2 \mathrm{e}^{-[E-E_j]^2/{\sigma_E}^2} \tag{S13}$$

where typically $t_\mathrm{fin} = 3T$ and $\sigma_E = 0.025\,\mathrm{eV}$. The sum over j is restricted to all states with the same angular momentum ℓ.

3.2 Velocity vs. length gauge

For comparison one can perform calculations in the length gauge by means of a similar method. The equations to be solved are

$$\mathrm{i}\dot{a}_j(t) = \sum_{j'} \left[E_j\delta_{jj'} - \tfrac{\mathrm{d}}{\mathrm{d}t}\mathcal{A}(t)\, d_{jj'}\right] a_{j'}(t), \tag{S14}$$

where $d_{jj'} = \frac{\ell}{\sqrt{4\ell^2-1}}\langle\varphi_j|r|\varphi_{j'}\rangle$ with $\ell = \max(\ell_j, \ell_{j'})$.

Figure S2 shows results of simulations with the largest partial wave ℓ_max included going well above what has been used before [1, 5–7]. It can be seen that even for $\ell_\mathrm{max} = 32$ the spectrum is not converged in the length gauge, while it only requires $\ell_\mathrm{max} = 1$ for convergence in the velocity gauge. One also recognizes the false dynamic interference appearing for low ℓ_max in the length gauge which is an artifact of the non-converged results. These non-converged results effectively mimic the behaviour of a system in which the continuum states undergo no stark shift; a direct consequence of the lack of enough partial waves required for accommodating the dependence of the stark shift of the continuum states on the ponderomotive energy in the length gauge. Obviously the effective Stark shift calculated using these results is wrong or more specifically it is exaggerated.

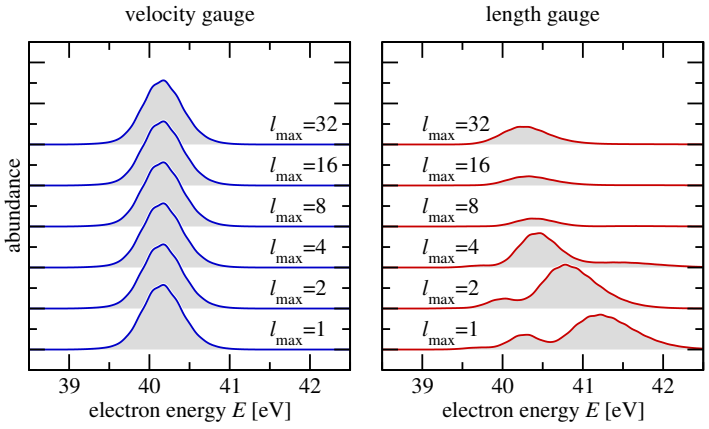

Figure S2: Comparison of photoelectron spectra obtained in the velocity and the length gauges for $T = 3\,\mathrm{fs}$, $I = 5{\times}10^{16}\mathrm{W/cm^2}$ and $\omega = 53.6\,\mathrm{eV}$.

References

[1] P. V. Demekhin and L. S. Cederbaum, *ac Stark effect in the electronic continuum and its impact on the photoionization of atoms by coherent intense short high-frequency laser pulses*. Phys. Rev. A 88, 043414 (2013).

[2] M. Gavrila, *Atomic structure and decay in high-frequency fields*. in *Atoms in intense laser fields*, edited by M. Gavrila (Academic Press, San Diego, 1992).

[3] M. H. Mittleman, *Introduction to the theory of laser-atom interactions* (Plenum Press, New York and London, 1993).

[4] R. Jackiw, *Quantum-mechanical sum rules*. Phys. Rev. 157, 1220 (1967).

[5] P. V. Demekhin and L. S. Cederbaum, *Dynamic interference of photoelectrons produced by high-frequency laser pulses*. Phys. Rev. Lett. 108, 253001 (2012).

[6] P. V. Demekhin, D. Hochstuhl, and L. S. Cederbaum, *Photoionization of hydrogen atoms by coherent intense high-frequency short laser pulses: Direct propagation of electron wave packets on large spatial grids*. Phys. Rev. A 88, 023422 (2013).

[7] C. Yu, N. Fu, G. Zhang, and J. Yao, *Dynamic Stark effect on XUV-laser-generated photoelectron spectra: Numerical experiment on atomic hydrogen*. Phys. Rev. A 87, 043405 (2013).